Journal of Computational Science 4 (2013) 71–79

Contents lists available at SciVerse ScienceDirect

Journal of Computational Science

journal homepage: www.elsevier.com/locate/jocs

Two phase simulations of glacier lake outburst flows☆

E. Bruce Pitman[a,*], Abani K. Patra[b], Dinesh Kumar[b], Kouichi Nishimura[c], Jiro Komori[c]

[a] Department of Mathematics, University at Buffalo, Buffalo, NY, United States
[b] Department of Mechanical and Aerospace Engineering, University at Buffalo, Buffalo, NY, United States
[c] Department of Earth and Environmental Sciences, Nagoya University, Nagoya, Japan

ARTICLE INFO

Article history:
Received 25 March 2012
Received in revised form 19 April 2012
Accepted 29 April 2012
Available online 25 May 2012

ABSTRACT

Natural moraines bounding glacial lakes can fail and cause floods called glacier lake outburst floods (GLOFs). Because of the volume of water released and the speed with which the outburst travels, GLOFs represent a serious hazard to downstream regions. Current ideas suggest the development and expansion of glacial lakes may be due to global warming, although this view is not universally accepted. In any event, people living downstream are exposed to significant hazard risk. For example, on October 7, 1994, the failure of the moraine at Lugge Lake in the Lunana region, Bhutan, caused a GLOF that killed more than 20 people. This paper presents a first attempt to understand the dynamics of GLOFs through numerical simulations, using a two phase model of fluid and granular material flows over natural terrain. These computations extend the TITAN2D simulation environment originally developed for volcanic hazard computations. By combining simulations and field studies, scientists can provide those charged with civil protection with better information with which to make preparations.

1. Introduction

Glacier lakes can be contained by moraines, which can fail and cause floods called glacier lake outburst floods (GLOFs). These GLOFs will contain water and granular material such as soil and small rocks, and can flow for many kilometers at high speed. As such GLOFs represent a serious hazard risk to regions downstream from the lake. For example, the October 7, 1994 failure of the moraine at Lugge Lake in the Lunana region, Bhutan, caused a GLOF that killed more than 20 people [4].

Combining field observations with numerical simulations can aid in understanding the hazard risk due to GLOFs. This paper presents a first attempt at developing a GLOF simulation tool, based on a two phase model of fluid and granular material [20]. The simulation environment extends the TITAN2D tool developed at the University at Buffalo [16,25]. TITAN2D simulates the mass flow of dry granular material, modeled as a Mohr–Coulomb material; because these mass flows are much longer (on the order of kilometers) than deep (on the order of 10 m), depth averaging is performed to obtain a system of partial differential equations for the flow thickness and momentum at every instant of time.

A key component of TITAN2D is the integration of digital elevation models (DEMs) which provide a representation of the terrain over which the mass flows. In the case of GLOFs, several issues are important to consider. First is the dynamics of glacier lake formation and growth. Second, a systematic study of the glacier melting process together with the related expansion of glacial lakes would inform modeling of the frequency of GLOFs. The failure process of moraines and the triggering of an outburst is not well understood. Finally, because glacier lakes are often located in high mountainous regions which are difficult to access for ground surveys, the accuracy of DEMs is suspect. We will not address these important questions in this paper. However the DEM issue is of particular concern here, and we make a brief detour to discuss its ramifications. Consider as a specific example typical geographic information systems for obtaining DEMs, such as ASTER or SRTM, which sample elevations at selected points perhaps every 30 m or 50 m (at best), usually in a somewhat arbitrary fashion, depending mostly on the flyover routes of the instrument. Importantly, the sample points do not account for the meandering of, say, a river valley. Thus different parts of the steep valley walls will be sampled, sometimes near the valley floor and at other times higher up the sidewalls. The resulting DEM appears to have large rises and falls in the valley floor. Needless to say, such a DEM must be corrected in order to accurately simulate the outburst flood.

It is important to also comment on the large range of scales in this problem and the consequent modeling error. The moving flood waters of a GLOF will often erode soil and entrain rocks during the flow. The soil particles are typically sub-centimeter sized, and rocks may range from centimeters to meters; the flows,

☆ This work has been supported in part by NSF grants 0620991, 0757367 and 0711497. Computing support from the Center for Computational Research at the University at Buffalo is gratefully acknowledged.

* Corresponding author. Tel.: +1 716 645 2711; fax: +1 716 645 3888.
E-mail addresses: pitman@buffalo.edu (E.B. Pitman), abani@buffalo.edu (A.K. Patra), dkumar@buffalo.edu (D. Kumar), knishi@nagoya-u.jp (K. Nishimura), j-k@e-mail.jp (J. Komori).

1877-7503/$ – see front matter © 2012 Published by Elsevier B.V.
http://dx.doi.org/10.1016/j.jocs.2012.04.007

sometimes as fast as tens of meters per second, propagate distances of tens of kilometers. This range of scales, and the complexity of the rheology describing the flowing mass, coupled with the mathematical problem of describing a free surface flow, makes modeling and computing GLOFs a significant challenge. This paper describes a first effort in modeling GLOFs that contain a mixture of liquid and granular materials. Our efforts try to strike a balance between fidelity to physics on the one hand and mathematical and computational tractability on the other.

2. Modeling

The origins of the modeling of dry avalanches is the pioneering work of Savage and Hutter [24]. They began with mass and momentum balance laws based on a Coulomb constitutive description of dry granular material. Making use of the small aspect ratio of typical flows, Savage and Hutter develop a "thin layer" model for granular flows down inclines. This work was later extended to two dimensions [6], and to flows over more general topography [5,16,19,21]. Hutter and colleagues [7] examine the appropriateness of these thin layer models for several different types of geophysical flows. Iverson [8] and later Iverson and Denlinger [9] argue that interstitial fluid alters the behavior of flows and must be included in the constitutive behavior of the flowing material. Based on the equations of mixture theory [2] these papers developed a system of mass and momentum balance laws for a mixture of liquid and granular material. However that modeling considered only the volume averaged mixture as the constituent material and an equation for the motion of pore fluid was not readily available. Instead Iverson and Denlinger postulated an advection–diffusion equation and fit coefficients to experimental data. An equation for the transport of fluid was postulated.

The work of [20] begins with the 2-fluid equations of motion as found in the engineering literature (e.g. [1,10]), which considers mass and momentum balance laws and phenomenologically modeled phase interaction terms. By combining depth averaging and physical approximations, a "thin-layer" model is developed for the solid–fluid mixture. The resulting equations constitute a system of hyperbolic PDEs, which, in the TITAN2D simulation environment, are solved by a parallel, adaptive grid method using a high-order Godunov solver [16]. Erosion has been modeled in dry granular systems [18,11], but has not been incorporated into two phase models. A principal input to TITAN2D is a digital elevation model (DEM) of the terrain over which the mixture may flow. TITAN2D accepts several DEM formats, and filters the input elevations to provide a method for finding the slope and curvature at every point, as required by the governing equations and the adaptive mesh. For other extensions of thin layer modeling in geophysical problems, see [13,14,17].

2.1. The 2-fluid model

The thin layer, two phase equations are derived in detail in Appendix; the interested reader should also consult [20]. Here we sketch the important notation and summarize the system of differential equations.

In three space dimensions, consider a thin layer of granular material and interstitial fluid, well mixed and each phase of constant specific density ρ^s and ρ^f, respectively, flowing over a smooth basal surface $b(x, y)$. Neglect any erosion of the basal surface. At any location, consider a Cartesian coordinate system $Oxyz$, with origin O defined so the plane Oxy is tangent to the basal surface and Oz the outward normal direction. As noted in [9], in considering flow over variable terrain, there should be no preferential direction in the xy-plane. Write $\mathbf{v}$, $\mathbf{u}$ for the velocities of the solid and fluid constituents, respectively, and φ for the solid volume fraction. When writing equations in component form, we use superscripts to denote the component in the x, y or z direction.

From [1], mass conservation for the two constituent phases may be written as

$$\partial_t \rho^s \varphi + \nabla \cdot (\rho^s \varphi \mathbf{v}) = 0 \tag{1}$$

$$\partial_t \rho^f (1-\varphi) + \nabla \cdot (\rho^f (1-\varphi)\mathbf{u}) = 0. \tag{1}$$

The momentum equations for the two species take the form

$$\rho^s \varphi(\partial_t \mathbf{v} + (\mathbf{v}\cdot\nabla)\mathbf{v}) = -\nabla\cdot\mathbf{T}^s - \varphi\nabla\cdot\mathbf{T}^f + \mathbf{f} + \rho^s\varphi\mathbf{g} \tag{2}$$

$$\rho^f (1-\varphi)(\partial_t \mathbf{u} + (\mathbf{u}\cdot\nabla)\mathbf{u}) = -(1-\varphi)\nabla\cdot\mathbf{T}^f - \mathbf{f} + \rho^f(1-\varphi)\mathbf{g}. \tag{2}$$

Here $\mathbf{f}$ is the interaction force, and several forms are possible. The reader is referred to [10] for a discussion. We follow [1] and adopt a simple drag form (see also the discussion in [8])

$$\mathbf{f} = (1-\varphi)\beta(\mathbf{u}-\mathbf{v})$$

where

$$\beta = \frac{(\rho^s - \rho^f)\varphi g}{v_T (1-\varphi)^m}$$

is a phenomenological function based on the experimental results of Richardson and Zaki [23], v_T is the terminal velocity of a typical solid particle falling in the fluid under gravity, g is the magnitude of the gravitational force, and m is a Richardson and Zaki exponent related to the Reynolds number of the flow. This form of β was deduced from experiments where both solid and fluid volume fractions were kept away from the 0–1 extremes; for our modeling, we cut off the unboundedness of the drag as $\varphi \to 1$.

Scale the x and y dimensions by a characteristic horizontal lengthscale L, the z direction by a typical flow thickness, H, time by $\sqrt{L/g}$, and set $\epsilon = H/L$. We assume the granular material is a Mohr–Coulomb plastic solid, with frictional boundary condition on b. We assume the fluid is inviscid, but exerts a drag at the basal surface, modeled as Navier slip at b, which accounts for all fluid dissipation. After depth averaging, and with several simplifying assumptions (see [20]), we arrive at the governing equations given as:

Total mass balance:

$$\partial_t \hat{h} + \partial_x(\hat{h}(\overline{\varphi v^x} + (1-\overline{\varphi})\overline{u^x})) + \partial_y(\hat{h}(\overline{\varphi v^y} + (1-\overline{\varphi})\overline{u^y})) = 0. \tag{3}$$

Here the depth averaged velocities are given by $\hat{h}\overline{v^x} = \int_b^h v^x\,dz$ and analogous expressions for the other components $\overline{v^y}$, $\overline{u^x}$, $\overline{u^y}$ and $\overline{\varphi}$. We have defined $\hat{h} = h - b$.

Solid mass balance:

$$\partial_t(\hat{h}\overline{\varphi}) + \partial_x(\hat{h}\overline{\varphi}\overline{v^x}) + \partial_y(\hat{h}\overline{\varphi}\overline{v^y}) = 0. \tag{4}$$

Solid x-momentum:

$$\begin{aligned}
&\partial_t(\hat{h}\overline{\varphi}\overline{v^x}) + \partial_x(\hat{h}\overline{\varphi}\overline{v^x v^x}) + \partial_y(\hat{h}\overline{\varphi}\overline{v^x v^y}) \\
&\quad = -\frac{1}{2}\epsilon\left(1-\frac{\rho^f}{\rho^s}\right)\partial_x(\alpha_{xx}\hat{h}^2\overline{\varphi}(-g^z)) \\
&\quad -\frac{1}{2}\epsilon\left(1-\frac{\rho^f}{\rho^s}\right)\partial_y(\alpha_{xy}\hat{h}^2\overline{\varphi}(-g^z)) \\
&\quad +\left(1-\frac{\rho^f}{\rho^s}\right)(-\epsilon\alpha_{xx}\partial_x b - \epsilon\alpha_{xy}\partial_y b + \alpha_{xz})\hat{h}\overline{\varphi}(-g^z) \\
&\quad -\frac{1}{2}\epsilon\frac{\rho^f}{\rho^s}\overline{\varphi}\partial_x(\hat{h}^2(-g^z)) - \epsilon\frac{\rho^f}{\rho^s}\hat{h}\overline{\varphi}(-g^z)\partial_x b
\end{aligned}$$

$$+\left(1-\frac{\rho^f}{\rho^s}\right)\frac{\hat{h}(1-\overline{\varphi})\overline{\varphi}}{\nu_T(1-\overline{\varphi})^m}(\overline{u^x}-\overline{v^x})+\hat{h}\overline{\varphi}g^x. \tag{5}$$

Solid y-momentum:

$$\begin{aligned}&\partial_t(\hat{h}\overline{\varphi}\overline{v^y})+\partial_x(\hat{h}\overline{\varphi}\overline{v^x v^y})+\partial_y(\hat{h}\overline{\varphi}\overline{v^y v^y})\\&=-\frac{1}{2}\epsilon\left(1-\frac{\rho^f}{\rho^s}\right)\partial_x(\alpha_{xy}\hat{h}^2\overline{\varphi}(-g^z))\\&-\frac{1}{2}\epsilon\left(1-\frac{\rho^f}{\rho^s}\right)\partial_y(\alpha_{yy}\hat{h}^2\overline{\varphi}(-g^z))\\&+\left(1-\frac{\rho^f}{\rho^s}\right)(-\epsilon\alpha_{xy}\partial_x b-\epsilon\alpha_{yy}\partial_y b+\alpha_{yz})\hat{h}\overline{\varphi}(-g^z)\\&-\frac{1}{2}\epsilon\frac{\rho^f}{\rho^s}\overline{\varphi}\partial_y(\hat{h}^2(-g^z))-\epsilon\frac{\rho^f}{\rho^s}\hat{h}\overline{\varphi}(-g^z)\partial_y b\\&+\left(1-\frac{\rho^f}{\rho^s}\right)\frac{\hat{h}(1-\overline{\varphi})\overline{\varphi}}{\nu_T(1-\overline{\varphi})^m}(\overline{u^y}-\overline{v^y})+\hat{h}\overline{\varphi}g^y.\end{aligned} \tag{6}$$

The earth pressure relation for the solid phase is employed, and basal shear stresses are assumed to be proportional to the normal stress:

$$T^{s*z}=-\frac{v^*}{||\mathbf{v}||}\tan(\phi_{bed})T^{szz}\equiv\alpha_{*z}T^{szz},$$

where * can be either x or y, and the velocity ratio determines the force opposing the motion in the *-direction, to the extend that force is mobilized [6,16] in that direction. Thus sliding velocity and basal traction are colinear. The α notation will provide a convenient shorthand. Likewise the diagonal stresses are taken to be proportional to the normal solid stress

$$T^{s**}=k_{ap}T^{szz}\equiv\alpha_{**}T^{szz},$$

where the same index x or y is used in both *s. Finally, following [9], xy shear stresses are determined by a Coulomb relation

$$T^{sxy}=-\mathrm{sgn}(\partial_y v^x)\sin(\phi_{int})k_{ap}T^{szz}\equiv\alpha_{xy}T^{szz},$$

where the sgn function ensures that friction opposes straining in the (x, y)-plane. The earth pressure coefficient is defined as

$$k_{ap}=2\frac{1\pm[1-\cos^2(\phi_{int})[1+\tan^2(\phi_{bed})]]^{1/2}}{\cos^2(\phi_{int})}-1.$$

Here we have assumed a Mohr–Coulomb constitutive relation for the flowing granular material, with an internal friction angle ϕ_{int} and a basal friction angle ϕ_{bed}. These angles determine the frictional dissipation of the material as it deforms internally, and as it shears over the fixed basal surface.

Fluid x-momentum:

$$\begin{aligned}&\partial_t(\hat{h}\overline{u^x})+\partial_x(\hat{h}\overline{u^x u^x})+\partial_y(\hat{h}\overline{u^x u^y})=-\frac{1}{2}\epsilon\partial_x\hat{h}^2(-g^z)-\epsilon\nu(\overline{u}^x\partial_x b)\\&-\left(\frac{1-(\rho^f/\rho^s)}{\rho^f/\rho^s}\right)\frac{\hat{h}\overline{\varphi}}{\nu_T(1-\overline{\varphi})^m}(\overline{u^x}-\overline{v^x})+\hat{h}g^x.\end{aligned} \tag{7}$$

Fluid y-momentum:

$$\begin{aligned}&\partial_t(\hat{h}\overline{u^y})+\partial_x(\hat{h}\overline{u^x u^y})+\partial_y(\hat{h}\overline{u^y u^y})=-\frac{1}{2}\epsilon\partial_y\hat{h}^2(-g^z)-\epsilon\nu(\overline{u}^y\partial_y b)\\&-\left(\frac{1-(\rho^f/\rho^s)}{\rho^f/\rho^s}\right)\frac{\hat{h}\overline{\varphi}}{\nu_T(1-\overline{\varphi})^m}(\overline{u^y}-\overline{v^y})+\hat{h}g^y.\end{aligned} \tag{8}$$

In deriving these equations we have integrated the fluid stresses $\int_b^h T^{fx*}\,dz$ to derive the slip dissipation, and then set to zero the depth-averaged viscous dissipation in the fluid interior. If the fluid viscosity μ is not large, fluid shearing contributes only a small amount to the momentum balance and Navier slip, with slip coefficient ν, is the dominant dissipative mechanism. Making this assumption retains the hyperbolicity of the resulting system, and avoids the mathematical and computational complexity of numerically solving an incompletely parabolic system of equations.

For completeness we also provide the z-momenta, which are recovered from the dynamic equations:

Fluid z-momentum:

$$\overline{T}^{fzz}(x,y)=(-g^z)\frac{\hat{h}}{2}. \tag{9}$$

Solid z-momentum:

$$\partial_z T^{szz}=\left(1-\frac{\rho^f}{\rho^s}\right)g^z\varphi=\left(1-\frac{\rho^f}{\rho^s}\right)\varphi\partial_z T^{fzz}. \tag{10}$$

These model equations constitute a system of six equations in the variables $\hat{h}$, $\hat{h}\overline{\varphi}$ and the four momenta $\hat{h}\overline{\varphi}$v and $\hat{h}(1-\overline{\varphi})$u (the ˜ denoting the depth-averaged x- and y-components of the velocities). Notice because of the weighting of the fluid stress term in the solid momentum balance, the equations cannot be put in conservation form. The structure of the equations is symmetric upon interchange of the x- and y-coordinates. Of course, to highlight special features of the model, it is possible to derive other forms of the solid or fluid or mixture momentum equations by algebraic manipulations of the equations presented here. This system is hyperbolic, under common conditions [20]. Together with initial and boundary conditions, the system constitutes a well-posed set of equations describing a 2-fluid, depth averaged, thin layer system.

2.2. Reduced model

The 2-fluid model described above assumes the interstitial fluid is inviscid, the only stress being a pressure. The model does include inertial effects in the fluid momentum equations. If fluid motion relative to the solid motion is not large [8], and if pressure is the only fluid stress considered, one might consider a Darcy-like approximation. Dropping the fluid inertia terms, the momentum equations in the x and y directions reduce to the pair

$$\begin{aligned}&\left(\frac{1-(\rho^f/\rho^s)}{\rho^f/\rho^s}\right)\frac{\hat{h}\overline{\varphi}}{\nu_T(1-\overline{\varphi})^m}(\mathrm{u}-\mathrm{v})-\epsilon\nu\mathrm{u}\nabla b\\&=-\frac{1}{2}\epsilon\nabla\hat{h}^2(-g^z)\mathbf{I}+\hat{h}\mathrm{g}.\end{aligned} \tag{11}$$

This pair of equations replaces the fluid momentum equations above; one should view this reduced system as a set of four evolution equations for $\hat{h}$, $\hat{h}\overline{\varphi}$, and $\hat{h}\overline{\varphi}$v. Given $\tilde{\mathbf{v}}$, (11) is then an equation for $\tilde{\mathbf{u}}$.

Eq. (11) for $\tilde{\mathbf{u}}$ contains derivatives of $\hat{h}$. When substituting u back into the total mass conservation equation, a derivative of $\tilde{\mathbf{u}}$ appears, leading to second derivatives of $\hat{h}$ (see [27]). Other equations contain only first derivative terms. A simple calculation indicates that the coefficient matrices of the first order derivative terms retain a hyperbolic structure. Thus the reduced model can be considered as degenerate parabolic, but the reduced model system is a well posed evolution system once appropriate initial and boundary conditions are assigned.

3. GLOF simulations

Here we report on preliminary results of simulations using the two phase model just presented, to reproduce the outburst flood at Lugge Lake in Bhutan. In this very mountainous region with steep valley walls, common and readily available DEMs did not sample

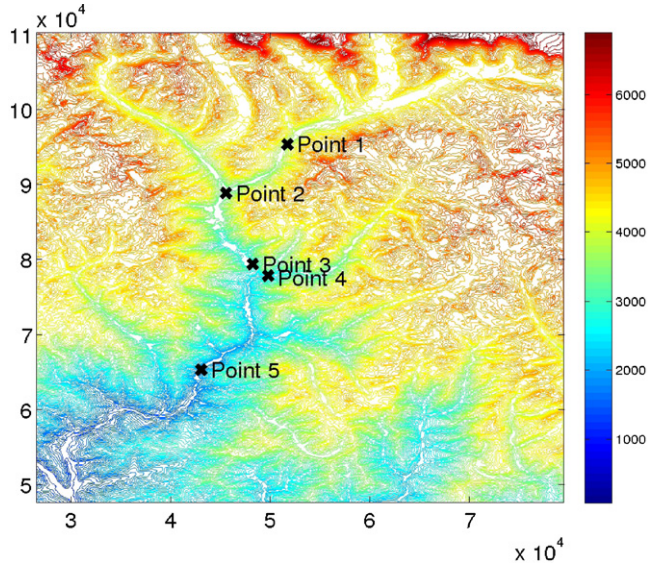

Fig. 1. A map of the region near Lugge Lake, Bhutan, with elevations indexed by color, and showing 5 locations at which computationally determined hydrographs have been sampled. The original terminus of the glacier lake is at the far northeast corner of the map, upstream from Point 1.

the valley floor directly. We corrected the DEMs by making use of hand-held GPS readings, to ensure the calculated elevation map makes sense.

The model equations constitute a hyperbolic system of balance laws which is solved using a Godunov method based on Davis' scheme [3]. An adaptive mesh algorithm is used, with refinements near the front of the propagating mass, at regions of rapid change in the dynamic variables, and wherever the topography experiences rapid changes. Mesh coarsening occurs where there is no flowing mass, and when the moving material varies slowly. Also we introduce additional modifications to resolve unphysical behaviors at the front; these mostly consist of additional levels of mesh refinement immediately at and ahead of the front, so the front always flows into a highly refined mesh cell. Parallel processing is used, using MPI calls. The reader should consult [16] for details.

We import a DEM of a region approximately 80 km × 60 km south and west of the lake; Fig. 1 provides a color-coded contour map of the region, showing the meandering of the riverbed and the steep slopes of the valley. Points 3 and 4 are close to one another—the valley makes a rapid descent between these points, accelerating the fluid–solid mixture. When running simulations, care must be exercised so the flow remains well behaved through this area.

As mentioned earlier, the model above does not account for bulking of the flow due to erosion. In two phase flows, erosion changes the solid volume fraction, which can dramatically affect the constitutive behavior of the flowing mass. To gain some insight into the flow behavior, Fig. 2 shows the maximum flow depth of a flows of pure fluid, and of mixtures of a 30% and 50% solid volume fraction, along the entire length of the river. The three plots compare the maximum depth for two different values of the Navier slip coefficient, $\nu = 0.075$ and $\nu = 0.15$.

To further illustrate the effect of dissipation on the mixtures, Fig. 3 shows the hydrographs at the five sample points, for three different solid volume fractions – 0% solids (i.e. pure fluid), and 30% and 50%. Results using the two different values of the slip coefficient are shown. The points 3 and 4 are near to each other; as the map suggests, the topography makes a marked change just below Point 3, and our interest in sampling at point 4 stems from the rapid changes in flow features that occur under some settings. In particular, flows without any fluid slip can experience rapid and sometimes unphysical accelerations at these locations unless exceptional care is taken in the simulation.

4. Conclusion

This paper models glacier lake outburst flows as a "thin layer" system of equations for a two phase mixture of a granular solid and an inviscid fluid. Navier slip is introduced to account for fluid dissipation. Simulations at Lugge Lake, Bhutan, provide a first attempt at modeling a GLOF using a two phase flow.

The Navier slip is a phenomenological coefficient, and simulations clearly demonstrate that its value can dramatically change runout distances and flow speeds. Among other uses, a Navier slip is used to approximate the no slip condition for the flow of a fluid over a rough surface by a slip condition applied to a smoother surface [15,12]. We have illustrated the model with two values of the slip coefficient, 0.075 and 0.15. These values are somewhat arbitrarily chosen. However these values are consistent with Coulomb basal friction angles of about 4° and 8°, which are likely near the minimum and maximum values of dissipation for a flowing liquid phase. Careful experimental calibration of the slip is needed in order to use this model for hazard predictions.

It is interesting to see that the volume fraction, when non-zero, plays only a small role in the front propagation speed and the overall features of the flow. In contrast, the difference between pure fluid and a fluid–solid mixture of even modest solid volume fraction is considerable and indicates the importance of including both phases when modeling. The choice of 30% and 50% volume fractions reflects typical solid fraction as seen in other breakout flows such as the 2007 crater lake lahar at Ruapehu, New Zealand. A more complete model that includes erosion of the basal soil and rock into the flowing glacier lake water will clarify the flow behavior.

Our results also highlight the need for accurate DEMs in the region under consideration.

This work demonstrates the robustness and flexibility of a two phase model for GLOFs, and the efficiency of our parallel, adaptive mesh solver for simulations.

Appendix A. Derivation of the 2-fluid model

In this Appendix we derive the governing two phase, thin layer equations, based on the 2-fluid model. Using the notation defined perviously, and based on [1], mass conservation for the two constituent phases may be written as

$$\partial_t \rho^s \varphi + \nabla \cdot (\rho^s \varphi \mathbf{v}) = 0 \tag{12}$$

$$\partial_t \rho^f (1-\varphi) + \nabla \cdot (\rho^f (1-\varphi)\mathbf{u}) = 0. \tag{12}$$

The momentum equations for the two species takes the form

$$\rho^s \varphi(\partial_t \mathbf{v} + (\mathbf{v}\cdot\nabla)\mathbf{v}) = -\nabla\cdot\mathbf{T}^s - \varphi\nabla\cdot\mathbf{T}^f + \mathbf{f} + \rho^s\varphi\mathbf{g} \tag{13}$$

$$\rho^f (1-\varphi)(\partial_t \mathbf{u} + (\mathbf{u}\cdot\nabla)\mathbf{u}) = -(1-\varphi)\nabla\cdot\mathbf{T}^f - \mathbf{f} + \rho^f(1-\varphi)\mathbf{g}. \tag{13}$$

We call attention to the volume fraction weighting of the stresses in (13), in contrast to modeling using mixture theory. The phase interaction force **f** was defined above.

Until now, no assumptions have been made about the constitutive behavior of the material, and specification of the stresses is still required. We will do so now. We must also specify boundary conditions for each phase. We assume the fluid is incompressible and Newtonian with a viscosity μ^f, and the solid material is a Mohr–Coulomb material, with an internal friction angle ϕ_{int}; see [24,20]. The full Coulomb relations are too complex to be used in a depth-averaged model and two simplifications are proposed. First, the proportionality (and alignment) of the tangential and normal forces that will be imposed as a basal boundary condition

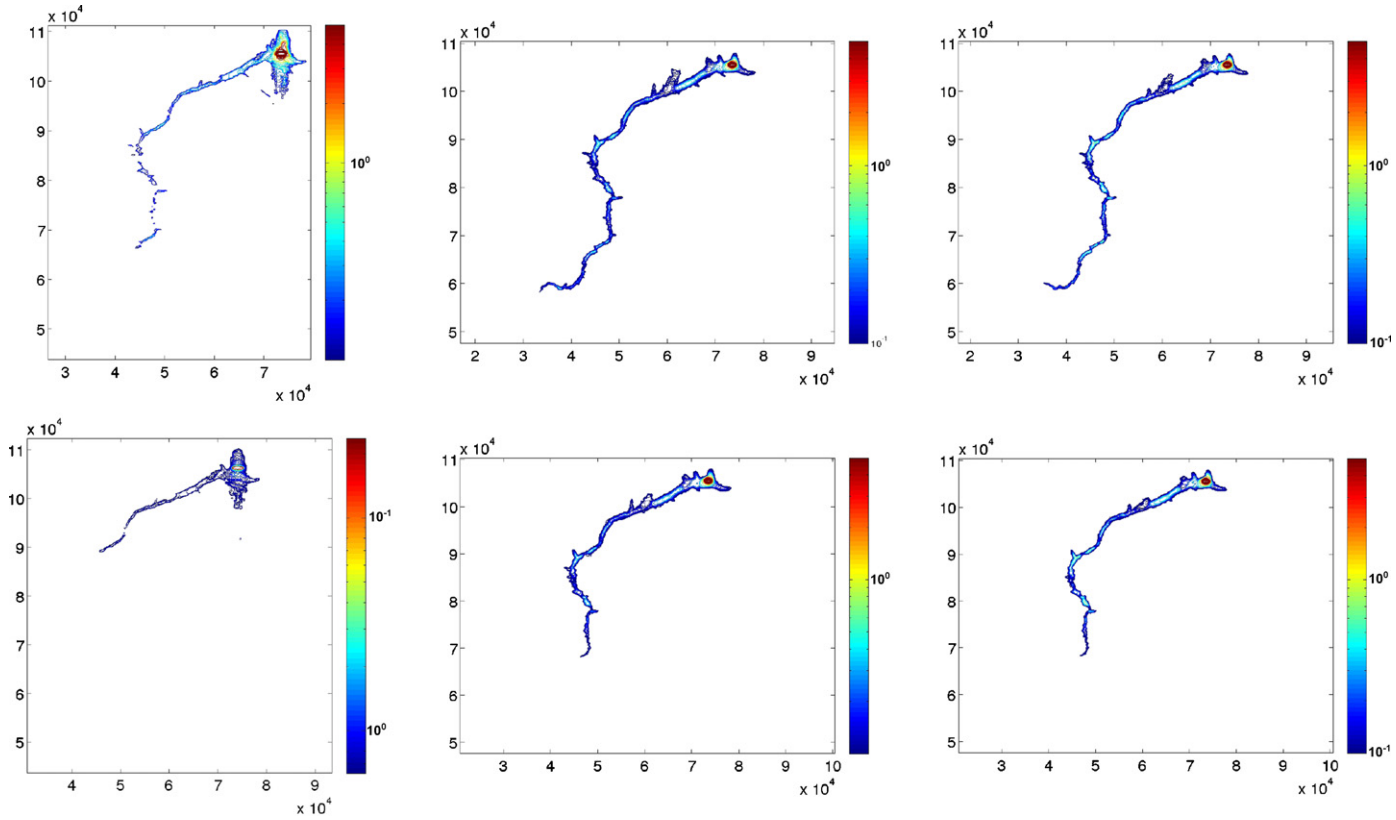

Fig. 2. Maximum flow depth of a pure fluid and 30 and 50% solid volume fraction flow, for two different values of the Navier slip coefficient – $\nu = 0.075$ (top), and $\nu = 0.15$ (bottom).

is assumed to hold throughout the thin flowing layer of material. Second, following Rankine [22] and Terzaghi [26], an earth pressure relation is assumed for the diagonal stress components, $T^{sxx} = k_{ap} T^{szz}$, where

$$k_{ap} = 2\frac{1 \pm [1 - \cos^2(\phi_{int})[1 + \tan^2(\phi_{bed})]]^{1/2}}{\cos^2(\phi_{int})} - 1.$$

Here the choice of the $\pm$ sign depends on whether flow is locally expanding (the active state, with $\nabla \cdot \mathbf{v} > 0$, and the $-$ sign) or contracting (the passive state, with $\nabla \cdot \mathbf{v} < 0$, and the $+$ sign). We assume the two phases are well mixed, and the upper free surface is a material surface and is stress free for both constituents. At the basal surface we assume frictional forces will be mobilized in both phases. For the solid phase this means that the flowing material and the basal surface interact via a bed friction angle ϕ_{bed}, and the principal directions of the stress and strain-rate are aligned. For the fluid phase we assume a simple Navier slip condition with slip coefficient ν.

Finally we comment that examination of the limiting cases of $\varphi = 1$ or $\varphi = 1$ must be performed with care. For example, to determine the limit equations for negligible fluid presence, not only must $\varphi \to 1$ but $\rho^f \to 0$ also. The reader may consult the discussion in [8,20].

At several junctures in the derivation below it is necessary to assume the depth average of a product of terms is the product of the depth averages. In particular, for some function f, we have occasion to approximate terms like $\overline{\varphi f}$ as $\overline{\varphi}\overline{f}$. It is possible to quantify the error made in this approximation; see [20].

A.1. Scaling

To proceed, we scale the equations. The characteristic length in the z-direction is H, and in x, y it is L. The timescale is taken to be $t^2 = L/g$. Typical stresses are on the order of the weight of material, so scale the solid stresses by $\rho^s gH$ and the fluid stress by $\rho^f gH$. After clearing the coefficients, the continuity equations for solids and fluid are unchanged. Several terms in the momentum equations are multiplied by $\epsilon = H/L$ which is small. Specifically, solids momentum balance in the x, y and z directions become

$$\begin{aligned}\varphi(\partial_t v^x + v^x \partial_x v^x + v^y \partial_y v^x + v^z \partial_z v^x) &= -(\epsilon \partial_x T^{sxx} + \epsilon \partial_y T^{sxy} + \partial_z T^{sxz}) \\ &- \frac{\rho^f}{\rho^s}\varphi(\epsilon \partial_x T^{fxx} + \epsilon \partial_y T^{fxy} + \partial_z T^{fxz}) \\ &+ \frac{(1 - (\rho^f/\rho^s))(1-\varphi)\varphi}{\nu_T (1-\varphi)^m}(u^x - v^x) + \varphi g^x \end{aligned} \tag{14}$$

$$\begin{aligned}\varphi(\partial_t v^y + v^x \partial_x v^y + v^2 \partial_y v^2 + v^z \partial_z v^y) &= -(\epsilon \partial_x T^{sxy} + \epsilon \partial_y T^{syy} + \partial_z T^{syz}) \\ &- \frac{\rho^f}{\rho^s}\varphi(\epsilon \partial_x T^{fxy} + \epsilon \partial_y T^{fyy} + \partial_z T^{fyz}) \\ &+ \frac{(1 - (\rho^f/\rho^s))(1-\varphi)\varphi}{\nu_T (1-\varphi)^m}(u^y - v^y) + \varphi g^y \end{aligned} \tag{15}$$

$$\begin{aligned}\epsilon\varphi(\partial_t v^z + v^x \partial_x v^z + v^y \partial_y v^z + v^z \partial_z v^z) &= -(\epsilon \partial_x T^{sxz} + \epsilon \partial_y T^{syz} + \partial_z T^{szz}) \\ &- \frac{\rho^f}{\rho^s}\varphi(\epsilon \partial_x T^{fxz} + \epsilon \partial_y T^{fyz} + \partial_z T^{fzz}) \\ &+ \frac{\epsilon(1 - (\rho^f/\rho^s))(1-\varphi)\varphi}{\nu_T (1-\varphi)^m}(u^z - v^z) + \varphi g^z \end{aligned} \tag{16}$$

In writing these equations, we have explicitly scaled the momentum interaction force, leaving a scaled parameter ν_T in the drag coefficient. Also, we note that components of gravity have been

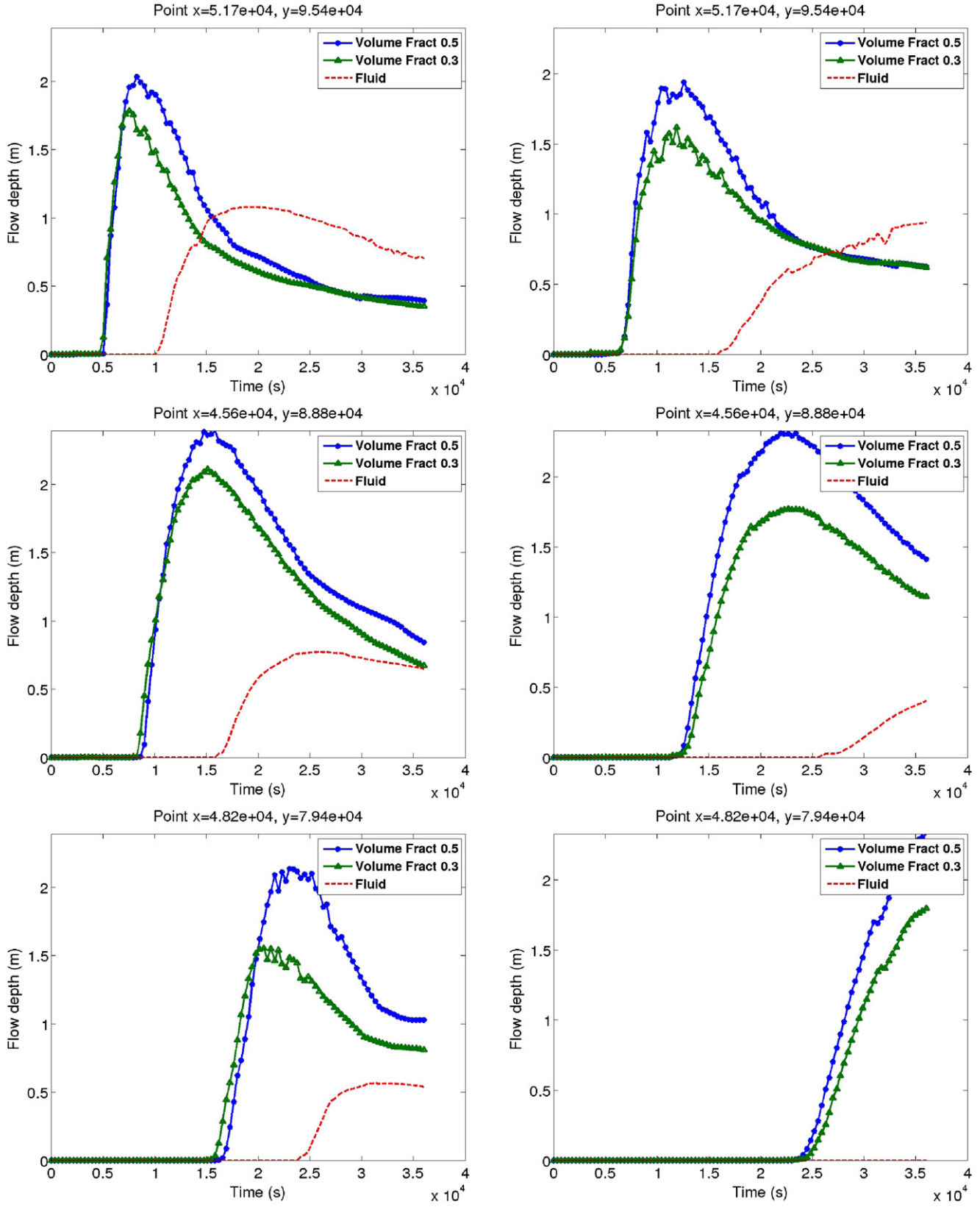

Fig. 3. Hydrographs at each of the five sampling locations (shown vertically), for flows of pure fluid and of a 30% and 50% volume fraction mixture. The left column of figures are for a slip coefficient of 0.075, the right for 0.15.

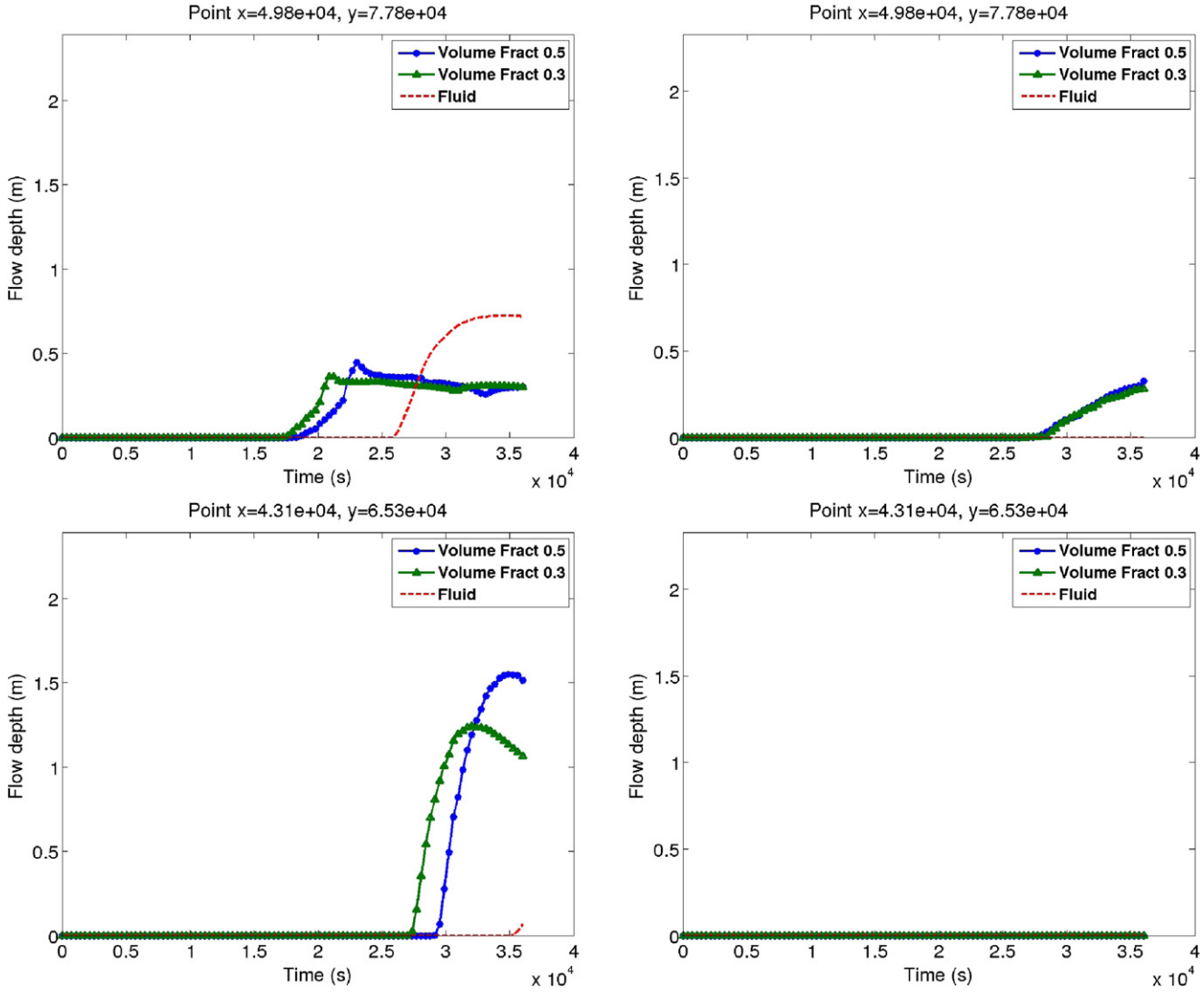

Fig. 3. (*continued*).

scaled by the magnitude g, so (g^x, g^y, g^z) is a unit vector. Usually one would drop all terms of order ϵ; again we refer the reader to [24] for a discussion of the need to retain the diagonal stress contributions. Because no preferential downslope direction is prescribed, and flow direction may change during a flow, we retain all the stress terms in both the x- and y-momentum equations, dropping only $O(\epsilon)$ terms in the z-direction; see the discussion in [9].

The fluid equations are likewise scaled:

$$\partial_t u^x + u^x\partial_x u^x + u^y\partial_y u^x + u^z\partial_z u^x = -(\epsilon\partial_x T^{fxx} + \epsilon\partial_y T^{fxy} + \partial_z T^{fxz}) - \frac{(1-(\rho^f/\rho^s))}{\rho^f/\rho^s}\frac{\varphi}{\nu_T(1-\varphi)^m}(u^x - v^x) + g^x \tag{17}$$

$$\partial_t u^y + u^x\partial_x u^y + u^y\partial_y u^y + u^z\partial_z u^y = -(\epsilon\partial_x T^{fxy} + \epsilon\partial_y T^{fyy} + \partial_z T^{fyz}) - \frac{(1-(\rho^f/\rho^s))}{\rho^f/\rho^s}\frac{\varphi}{\nu_T(1-\varphi)^m}(u^y - v^y) + g^y \tag{18}$$

$$\epsilon(\partial_t u^z + u^x\partial_x u^z + u^y\partial_y u^z + u^z\partial_z u^z) = -(\epsilon\partial_x T^{fxz} + \epsilon\partial_y T^{fyz} + \partial_z T^{fzz}) - \epsilon\frac{(1-(\rho^f/\rho^s))}{\rho^f/\rho^s}\frac{\varphi}{\nu_T(1-\varphi)^m}(u^z - v^z) + g^z \tag{19}$$

We note that different scaling for the solid and fluid momentum equations has produced phase interaction terms with different coefficients. Simply adding the component momentum equations will not result in the force terms canceling each other.

A.2. Mass balance

Adding together the solids and fluids mass balance equations, we find

$$\nabla\cdot(\varphi\mathbf{v} + (1-\varphi)\mathbf{u}) = 0.$$

That is, the volume-weighted mixture flow is incompressible. We now depth average this equation:

$$\int_b^h \nabla\cdot(\varphi\mathbf{v} + (1-\varphi)\mathbf{u})\,dz = 0. \tag{20}$$

Using the Leibniz rule to interchange differentiation and integration, and that the upper free surface is a material surface, we find an equation for the total mass of the solid and fluid

$$\partial_t\hat{h} + \partial_x(\hat{h}(\overline{\varphi}\overline{v^x} + (1-\overline{\varphi})\overline{u^x})) + \partial_y(\hat{h}(\overline{\varphi}\overline{v^y} + (1-\overline{\varphi})\overline{u^y})) = 0. \tag{21}$$

We would like to depth average the mass equation for the solid phase, but the lack of phase-specific boundary conditions would seem to preclude such an integration. By assuming the solid material satisfies the basal and upper surface conditions we derive a solids mass balance equation

$$\partial_t(\hat{h}\overline{\varphi}) + \partial_x(\hat{h}\overline{\varphi}\overline{v^x}) + \partial_y(\hat{h}\overline{\varphi}\overline{v^y}) = 0. \tag{22}$$

To be sure, the imposition of individual phase mass balance is an assumption that needs further validation; more specifically, the argument breaks down when the difference $\mathbf{v} - \mathbf{u}$ is not small. We refer the interested reader to [9,20] for a discussion.

A.3. z-momentum

Observe that, upon setting ϵ to zero in the fluid z-momentum equation, we find the fluid to be hydrostatic:

$$\partial_z T^{fzz} = g^z.$$

Integrating and imposing boundary conditions, we find

$$T^{fzz}(x, y, z) = (-g^z)[h - z] \tag{23}$$

and the average

$$\overline{T}^{fzz}(x, y) = (-g^z)\frac{\hat{h}}{2}. \tag{24}$$

In the same manner, the solid z-momentum becomes

$$\partial_z T^{szz} + \frac{\rho^f}{\rho^s}\varphi\partial_z T^{fzz} = \varphi g^z.$$

Substituting,

$$\partial_z T^{szz} = \left(1 - \frac{\rho^f}{\rho^s}\right) g^z\varphi = \left(1 - \frac{\rho^f}{\rho^s}\right)\varphi\partial_z T^{fzz}.$$

Thus the solid stress in the normal direction at any height is equal to the reduced weight of the solid material overburden.

Observe that, at this juncture, any contribution to the z-momentum from fluid shearing – terms like T^{fxz}, T^{fyz} – would be lost due to scaling. This observation suggests that, even with a viscosity μ, the pressure is the largest internal force contributing to the fluid stress, and the z-velocities can be neglected.

A.4. x- and y-momentum

Depth averaging the x- and y-momentum equations is complicated by the nonlinearities in the terms and the non-conservative product $\varphi\nabla\mathbf{T}^f$ in the solid momentum equation. For the solid equations we quote the results from [20]

Solid x-momentum:

$$\begin{aligned}
&\partial_t(\hat{h}\overline{\varphi}\overline{v^x}) + \partial_x(\hat{h}\overline{\varphi}\overline{v^x v^x}) + \partial_y(\hat{h}\overline{\varphi}\overline{v^x v^y})\\
&= -\frac{1}{2}\epsilon\left(1 - \frac{\rho^f}{\rho^s}\right)\partial_x(\alpha_{xx}\hat{h}^2\overline{\varphi}(-g^z))\\
&-\frac{1}{2}\epsilon\left(1 - \frac{\rho^f}{\rho^s}\right)\partial_y(\alpha_{xy}\hat{h}^2\overline{\varphi}(-g^z))\\
&+\left(1 - \frac{\rho^f}{\rho^s}\right)(-\epsilon\alpha_{xx}\partial_x b - \epsilon\alpha_{xy}\partial_y b + \alpha_{xz})\hat{h}\overline{\varphi}(-g^z)\\
&-\frac{1}{2}\epsilon\frac{\rho^f}{\rho^s}\overline{\varphi}\partial_x(\hat{h}^2(-g^z)) - \epsilon\frac{\rho^f}{\rho^s}\hat{h}\overline{\varphi}(-g^z)\partial_x b\\
&+\left(1 - \frac{\rho^f}{\rho^s}\right)\frac{\hat{h}(1-\overline{\varphi})\overline{\varphi}}{\nu_T(1-\overline{\varphi})^m}(\overline{u^x} - \overline{v^x}) + \hat{h}\overline{\varphi}g^x.
\end{aligned} \tag{25}$$

Solid y-momentum:

$$\begin{aligned}
&\partial_t(\hat{h}\overline{\varphi}\overline{v^y}) + \partial_x(\hat{h}\overline{\varphi}\overline{v^x v^y}) + \partial_y(\hat{h}\overline{\varphi}\overline{v^y v^y})\\
&= -\frac{1}{2}\epsilon\left(1 - \frac{\rho^f}{\rho^s}\right)\partial_x(\alpha_{xy}\hat{h}^2\overline{\varphi}(-g^z))\\
&-\frac{1}{2}\epsilon\left(1 - \frac{\rho^f}{\rho^s}\right)\partial_y(\alpha_{yy}\hat{h}^2\overline{\varphi}(-g^z))\\
&+\left(1 - \frac{\rho^f}{\rho^s}\right)(-\epsilon\alpha_{xy}\partial_x b - \epsilon\alpha_{yy}\partial_y b + \alpha_{yz})\hat{h}\overline{\varphi}(-g^z)\\
&-\frac{1}{2}\epsilon\frac{\rho^f}{\rho^s}\overline{\varphi}\partial_y(\hat{h}^2(-g^z)) - \epsilon\frac{\rho^f}{\rho^s}\hat{h}\overline{\varphi}(-g^z)\partial_y b\\
&+\left(1 - \frac{\rho^f}{\rho^s}\right)\frac{\hat{h}(1-\overline{\varphi})\overline{\varphi}}{\nu_T(1-\overline{\varphi})^m}(\overline{u^y} - \overline{v^y}) + \hat{h}\overline{\varphi}g^y.
\end{aligned} \tag{26}$$

We now proceed to derive an equation for the fluid motion. Depth averaging for the fluid presents fewer difficulties than in the solid equations.

Fluid x-momentum:

$$\begin{aligned}
&\partial_t(\hat{h}\overline{u^x}) + \partial_x(\hat{h}\overline{u^x u^x}) + \partial_y(\hat{h}\overline{u^x u^y}) = -\frac{1}{2}\epsilon\partial_x\hat{h}^2(-g^z) - \epsilon\nu(\overline{u}^x\partial_x b)\\
&-\left(\frac{1 - (\rho^f/\rho^s)}{\rho^f/\rho^s}\right)\frac{\hat{h}\overline{\varphi}}{\nu_T(1-\overline{\varphi})^m}(\overline{u^x} - \overline{v^x}) + \hat{h}g^x.
\end{aligned} \tag{27}$$

Fluid y-momentum:

$$\begin{aligned}
&\partial_t(\hat{h}\overline{u^y}) + \partial_x(\hat{h}\overline{u^x u^y}) + \partial_y(\hat{h}\overline{u^y u^y}) = -\frac{1}{2}\epsilon\partial_y\hat{h}^2(-g^z) - \epsilon\nu(\overline{u}^y\partial_y b)\\
&-\left(\frac{1 - (\rho^f/\rho^s)}{\rho^f/\rho^s}\right)\frac{\hat{h}\overline{\varphi}}{\nu_T(1-\overline{\varphi})^m}(\overline{u^y} - \overline{v^y}) + \hat{h}g^y.
\end{aligned} \tag{28}$$

References

[1] T.B. Anderson, R. Jackson, A fluid mechanical description of fluidized beds: equations of motion, Industrial and Engineering Chemistry Fundamentals 6 (1967) 527–539.
[2] A. Bedford, D.S. Drumheller, Recent advances: theories of immicible and structured mixtures, International Journal of Engineering Science 21 (1983) 863–960.
[3] S.F. Davis, Simplified second order Godunov type methods, SIAM Journal of Scientific and Statistical Computing 9 (1988) 445–473.
[4] K. Fujita, R. Suzuki, T. Nuimura, A. Sakai, Performance of ASTER and SRTM DEMs, and their potential for assessing glacial lakes in the Lunana region, Bhutan Himalaya, Journal of Glaciology 54 (2008) 220–228.
[5] J.M.N.T. Gray, M. Wieland, K. Hutter, Gravity-driven free surface flow of granular avalanches over complex basal terrain, Proceedings of the Royal Society of London Series A 455 (1999) 1841–1874.
[6] K. Hutter, M. Siegel, S.B. Savage, Y. Nohguchi, Two-dimensional spreading of a granular avalanche down an inclined plane; Part 1: Theory, Acta Mechanica 100 (1993) 37–68.
[7] K. Hutter, Y. Wang, S.P. Pudasaini, The Savage–Hutter Avalanche model: how far can it be pushed? Philosphical Transactions of the Royal Society A 363 (2003) 1507–1528.
[8] R.M. Iverson, The physics of debris flows, Reviews of Geophysics 35 (1997) 245–296.
[9] R.M. Iverson, R.P. Denlinger, Flow of variably fluidized granular material across three-dimensional terrain 1. Coulomb mixture theory, Journal of Geophysical Research 106 (2001) 537–552.
[10] R. Jackson, The Dynamics of Fluidized Particles, Cambridge University Press, 2000.
[11] L. Le, E.B. Pitman, A model for granular flows over an erodible surface, SIAM Journal of Applied Mathematics 70 (2009) 1407–1427.
[12] L.G. Leal, Advanced Transport Phenomena: Fluid Mechanics, Cambridge University Press, 2007.
[13] M.Y. Louge, S. Keast, On dense granular flows down flat frictional inclines, Physics of Fluids 13 (2001) 1213–1233.
[14] A. Mangeney-Castelnau, B. Bouchut, J.P. Vilotte, E. Lajeunesse, A. Aubertin, M. Pirulli, On the use of Saint–Venant equations for simulating the spreading of a granular mass, Journal of Geophysical Research 110 (2005) B09103.

[15] M.J. Miksis, S.H. Davis, Slip over rough and coated surfaces, Journal of Fluid Mechanics 273 (1994) 125–139.
[16] A.K. Patra, A.C. Bauer, C. Nichita, E.B. Pitman, A.K. Patra, M.F. Sheridan, M. Bursik, B. Rupp, A. Weber, A. Stinton, L. Namikawa, A. Renschler, Parallel adaptive numerical simulation of dry avalanches over natural terrain, Journal of Volcanology and Geophysical Research 139 (2005) 1–21.
[17] M. Pelanti, F. Bouchut, A. Mangeney, A Roe-type scheme for two-phase shallow granular flows over variable topography, Mathematical Modelling and Numerical Analysis (ESAIM:M2AN) 42 (2008) 851–885.
[18] E.B. Pitman, C. Nichita, A. Patra, A.C. Bauer, M. Bursik, A. Webber, A numerical study of granular flows on erodible surfaces, Discrete and Control Dynamical Systems – Series B 3 (2003) 589–599.
[19] E.B. Pitman, A. Patra, A. Bauer, C. Nichita, M. Sheridan, M. Bursik, Computing debris flows, Physics of Fluids 15 (2003) 3638–3646.
[20] E.B. Pitman, L. Le, A two-fluid model for avalanche and debris flows, Philosphical Transactions of the Royal Society A 363 (2005) 1573–1601.
[21] S.P. Pudasaini, K. Hutter, Rapid shear flows of dry granular material down curved and twisted channels, Journal of Fluid Mechanics 495 (2003) 193–208.
[22] W.J.M. Rankine, On the stability of loose earth, Philosphical Transactions of the Royal Society 147 (1857) 9–27.
[23] J.F. Richardson, W.N. Zaki, Sedimentation and fluidization: Part I, Transactions of the Institute of Chemical Engineering 32 (1954) 35–53.
[24] S.B. Savage, K. Hutter, The motion of a finite mass of granular material down a rough incline, Journal of Fluid Mechanics 199 (1989) 177–215.
[25] M.F. Sheridan, A.J. Stinton, A.K. Patra, E.B. Pitman, A.C. Bauer, C.C. Nichita, Evaluating TITAN2D mass-flow model using the 1963 Little Tahoma Peak avalanches, Mount Rainier, Washington, Journal of Volcanology and Geothermal Research 139 (2005) 89–102.
[26] K. Terzaghi, The shearing resistance of saturated soils and the angle between planes of shear, in: Proceedings of the 1st International Conference on Soil Mechanics, 1936, pp. 54–56.
[27] D. Zhang, A. Prosperetti, Momentum and energy equations for dispersed two phase flows and their closure for dilute suspensions, International Journal of Multiphase Flow 23 (1997) 425–453.

E. Bruce Pitman received his Ph.D. in mathematics from Duke University in 1985. After post-doctoral appointments at the Courant Institute at New York University and the Institute for Mathematics and its Applications, and an appointment at the New Jersey Institute of Technology, he came to the University at Buffalo in 1989. He served as Vice Provost for Educational Technology, and Associate Dean for Research and Sponsored Programs before being named Dean of the College of Arts and Sciences in 2011.

Abani K. Patra earned his Ph.D. in 1995 from the Computational and Applied Mathematics program at the University of Texas at Austin. He joined the faculty in Mechanical and Aerospace Engineering at Buffalo in 1996. An NSF Career Award winner, he was Program Director at NSF in the Office of Cyber infrastructure from 2007 to 2010.

Dinesh Kumar is a graduate student in the Department of Mechanical and Aerospace Engineering at the University at Buffalo. He has worked on the TITAN2D computing environment, for simulations of geophysical mass flows, on two phase flows, and on SHP methods for mass flows.

Kouichi Nishimura earned his Doctor of Science from Hokkaido University in 1990. He held visiting appointments at Cambridge University and at Sandia National Labs, and an appointment at the National Research Institute for Earth Science and Disaster Prevention before becoming a professor at Niigata. He moved to Nagoya University in 2008.

Jiro Komori is a graduate student in the Earth and Environmental Sciences department at Nagoya. He has spent much of the last three years in Bhutan studying the topography and geology of glacier lakes and the surrounding regions.